Geological Quarterly, 2012, **56** (4): 665–680
DOI: http://dx.doi.org/10.7306/gq.1048

Statistical analysis of petrophysical parameters of Middle Miocene rocks from the Polish Carpathian Foredeep

Maria BAŁA, Jadwiga JARZYNA and Zofia MORTIMER

Bała M., Jarzyna J. and Mortimer Z. (2012) – Statistical analysis of petrophysical parameters of Middle Miocene rocks from the Polish Carpathian Foredeep. Geol. Quart., **56** (4): 665–680, doi: 10.7306/gq.1048

Middle Miocene – Sarmatian thin-bedded sandstone and shales of southern Poland have been a subject of statistical studies to differentiate between good and poor reservoir rocks and to show gas-saturated layers in comparison to water-saturated strata. Statistical studies including fractal analysis were performed on well logging data from the Sędziszów 34 borehole drilled in a belt of hydrocarbon deposits that continue below the northern edge of the Carpathian–Stebnik overthrust. Lithological variability and porosity differentiation and changes in water saturation were traced on the basis of the results of well logging interpretation. Basic statistics and histograms of petrophysical parameters have been analysed. A generalized second order fractal correlation dimension was calculated for all parameters and analysed as for a time series. Fractal dimensions did not correlated with the parameters, but good positive correlations between them and the parameters were observed and showed that the curves analysed had the same type of complexity. High correlation coefficients showed pairs of fractal dimensions for those parameters which had similar variability and the same curve roughness. The fractal correlation dimension described the type of complexity of the parameter (curve roughness) and indicated, for example, how shaliness influenced the reservoir properties of the local Middle Miocene. Therefore, the results were also useful in practice, which gave extra information on thin-bedded reservoir rocks.

Maria Bała, Jadwiga Jarzyna and Zofia Mortimer, Faculty of Geology Geophysics and Environmental Protection, Department of Geophysics, AGH University of Science and Technology, Mickiewicza 30, 30-059 Kraków, Poland, e-mails: bala@geol.agh.edu.pl, jarzyna@agh.edu.pl, mortimer@geol.agh.edu.pl (received: April 5, 2012; accepted: May 25, 2012; first published online: October 19, 2012).

Key words: reservoir rocks, Middle Miocene, Carpathian Foredeep, fractal analysis, statistical analysis, well logging data.

INTRODUCTION

The Polish Carpathian Foredeep has been regarded as a prospective area since the first discoveries of gas fields there at the end of 19th century. The foreland successions accumulated high-methane gas deposits mostly in the Middle Miocene (Badenian and Sarmatian) strata (Karnkowski, 1999; Oszczypko et al., 2006; Kotarba et al., 2011; Oszczypko and Oszczypko-Clowes, 2012). A long tradition of successful prospecting for gas in the Carpathian Foredeep was based on studies of seismic structural traps and seismic anomalies related to tectonic events (Karnkowski, 1994; Krzywiec et al., 2005). In the mid- 1990s special attention was paid to non-standard seismic correlation lines related to structural anomalies frequently met in the Miocene succession and to Direct Hydrocarbon Indicators (Borys and Myśliwiec, 2002; Myśliwiec, 2004a; Myśliwiec et al., 2004a, b).

Since the very beginning, well logging data were used for depth matching of structural seismic results and recognition of petrophysical parameters (Karnkowski, 1999; Pietsch et al., 2007; Krzywiec et al., 2008). Information on sedimentary environment and facies has also been obtained from well logging (Porębski, 1996; Myśliwiec, 2006; Krzywiec et al., 2008). Porosity and permeability and water saturation have always been the most important properties to engineers, who use these to select stratigraphic intervals to be exploited (Bala, 2011). However, the well test outcomes were not always in agreement with results of well logging data interpretation because the geological structure of heterogeneous thin-bedded sandstone–mudstone–claystone Sarmatian deposits with individual bed thicknesses of a dozen or so centimeters caused errors in well logging records, because the vertical resolution of the standard devices is lower than bed thickness. Standard resistivity logs (normal and lateral), considered in the past as the most important source of information on water/gas saturation, generated the highest discrep-

ancies between the true resistivity of the thin sandstone beds and measured apparent resistivity provided by logs. A "masking effect" in apparent resistivity was clearly observed (Zorski, 2009). Since the High Resolution Array Induction device (HRAI) was included into well logging measurements, interpreted results of water/gas saturation were better but in many cases HRAI measurements were not sufficient to obtain the true resistivity of thin gas-saturated layers. A special methodology was developed to improve gas saturation (Zorski, 2009) but petrophysicists and well log analysts remained interested in improving the methodology of identification of gas-saturated thin layers.

It was remarkable that it was not only clean sandstones that were gas reservoirs in the Sarmatian deposits. Frequently, high inflow was observed from highly shaly sandstones (Myśliwiec, 2004b). Since thinly bedded formations were considered as the largest source of global hydrocarbon production, any improvement in the methodology of determining sandstone/sand volume and calculating proper net to gross value are extremely valuable. Attention was focused on each new or modified method for classifying such a unit in order to select layers having good reservoir parameters that increased the productivity of these reservoirs. This paper provides a methodology that delivers more information from well logging by applying statistical analysis and a fractal approach.

In the last years, fractal analysis applied to a characterize a rock formation on the basis of well logs has been considered by several authors. They discussed this approach in many respects but the common motive was self-similarity detectable in well logs and used in solving geological tasks in which well logging delivered essential knowledge. Papers that focused on lithological identification (Álvarez et al., 2003; Lopez and Aldana, 2007) and porosity and permeability determination (Pape et al., 1999) were regarded as the most representative examples of efficient use of fractal analysis. Laboratory data from the sandstones and shales of the Middle Miocene of the Polish Carpathian Foredeep were classified into groups of various reservoir parameters on the basis of the fractal dimension by Such (1998, 2004). In this paper, fractal analysis has been performed on conventional log signals represented as one-dimensional depth series. From this point of view, we simply considered the log as a digitized curve, along which the relative variation of geometrical and statistical characteristics were analysed independently of the absolute scaling of parameters. One-dimensional depth series in our case were processed similarly to one-dimensional time series. The simple statistics of the raw data were an important part of this approach.

Statistical studies including fractal analysis were performed using well logging data and results of their comprehensive interpretation from the Sędziszów 34 borehole which was drilled in an extensive belt of hydrocarbon deposits continuing below the Carpathian–Stebnik overthrust along its northern edge (Fig. 1). The studies encompassed the Sarmatian succession from the depth interval of 1300–2931 m.

GEOLOGICAL SETTING

The Sędziszów 34 borehole penetrated the multi-horizon gas field of Zagorzyce located in the middle part of the Carpathian Foredeep south of the Czarna Sędziszowska deposit and south-west of the Palikówka deposit (Fig. 1). Going from the top of the geological profile, interbedded shales and sandstones typical of the Carpathian Foredeep below the Carpathian–Stebnik overthrust were drilled, and the claystones and heterolithic deposits of the Stebnik Unit, and towards the bottom of the borehole, an alternating succession of Middle Miocene sandstones, mudstones and claystones as well as Carboniferous limestone bedrock were identified (Table 1). The autochthonous Miocene Sarmatian and Badenian succession of the study area comprises claystones, mudstones and sandstones. The Sarmatian succession consists of such deposits interbedded on a scale of several centimetres. Badenian anhydrite and gypsum were observed sporadically. The Middle Miocene of the Zagorzyce deposit area rests on Jurassic and Carboniferous rocks although Jurassic deposits were not observed in Sędziszów 34 borehole.

WELL LOGGING DATA

In 2009, Geofizyka Kraków Ltd. carried out well logging with the use of Halliburton equipment and domestic CAG equipment. Measurements covered a depth interval of 1300–2931 m for which results of the comprehensive interpretation were made available (Documentation of the Sędziszów 34 borehole, 2009). Parameters shown in Table 2 were used in fractal studies of correlation dimension. Measurements and interpretation were made with a depth step of 0.1 m.

LITHOLOGICAL VARIABILITY OF THE MIDDLE MIOCENE

To illustrate the variability of thin-bedded Middle Miocene strata we show some results of the comprehensive interpretation made by POGC Warsaw, Sanok Branch, Jasło Office (2009) in terms of evaluation of mineral composition, porosity, water- and gas-saturation, and rock permeability at the depth interval of 1875–2000 m (Fig. 2). The content of sandstones and shales was strongly variable. Great variations in porosity and saturation and permeability were also detected.

Frequency histograms were also calculated to show the variability of geophysical parameters measured for a depth interval of the Sarmatian. The Gaussian distribution line was drawn in all histograms to show that the distributions were similar to normal (Figs. 3 and 4). One could see a great variability of interval transit time (DT) and bulk density (RHOB) and natural gamma radioactivity (GRC) (Fig. 3). The values of DT ranged from 225–385 μs/m; the dominant value of 305 μs/m provided an evidence for considerable shaliness of the study formations. Bulk density ranged from 2.00 to 2.71 g/cm^3. The shape of the histogram showed a dominance of samples with higher values with a range of 2.51–2.61 g/cm^3. The GRC histogram was also shifted towards higher values. The greatest class size ranged from 70.4 to 95.8 API, with a maximum value of 124.8 API.

The comprehensive look at three histograms in Figure 3 showed that the interval transit time distribution was closest to a

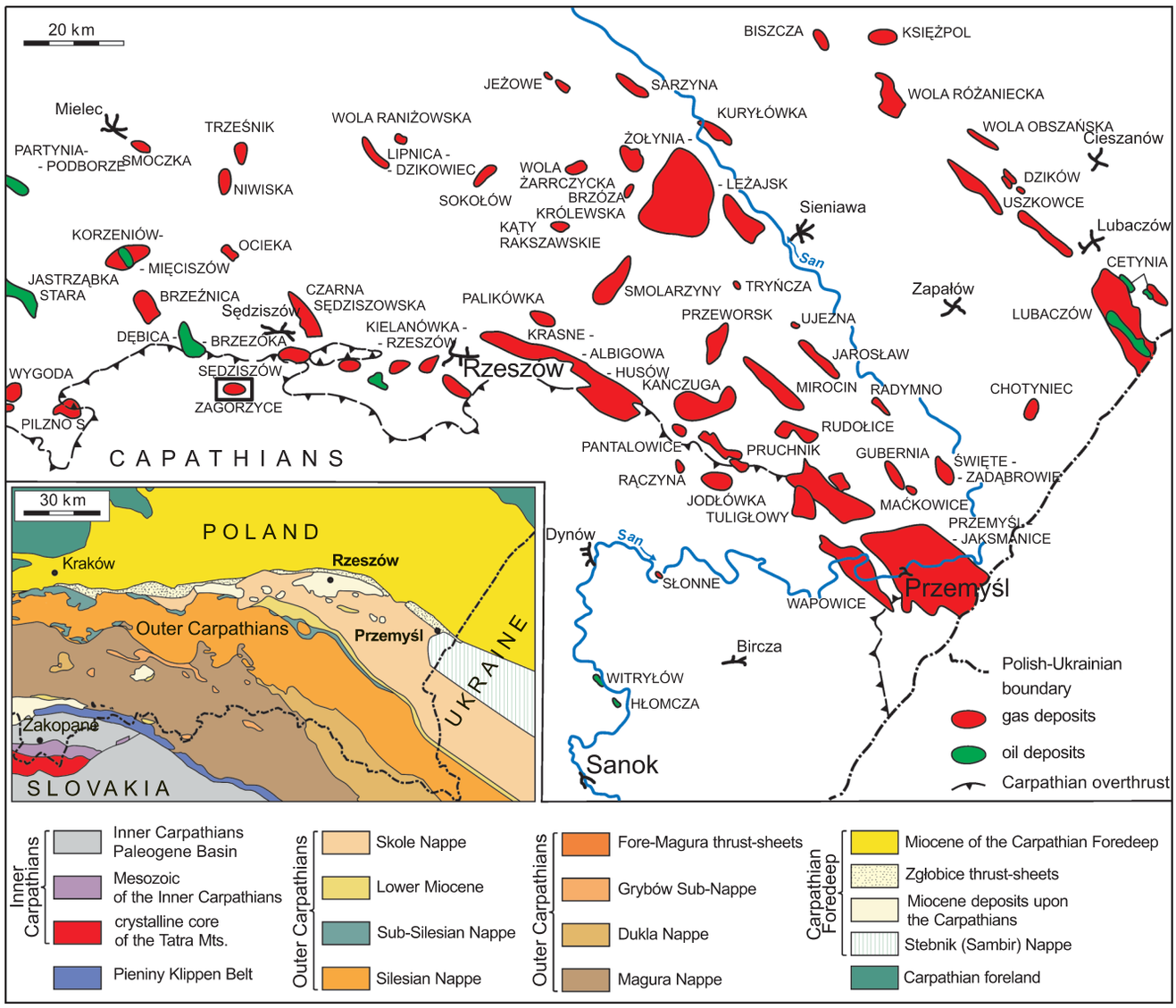

Fig. 1. Location of the Sędziszów gas deposit in the Carpathian Foredeep (Karnkowski, 1999; Oszczypko, 1998, modified)

normal distribution while the two other were skewed in relation to the Gaussian distribution. The DT distribution showed that the effects of mineral composition (including shaliness) and media filling the pore space on the shape of the DT anomalies were similar. This was supported by the porosity histogram (Fig. 4) in which one could see that PHI samples from a range of 0–15% have similar size, except the 1.39–3.38% class which that increased shaliness decreased sandstone porosity. Two other histograms suggested a dominance of clay minerals with density greater than 2.51 g/cm^{3}such as illite. The Th vs. K cross-plot (Fig. 5) supported this interpretation. In the Figure 5 plot, illite dominated; some data points identified likely micas in the sandstones.

Frequency histograms were also calculated for results of the comprehensive interpretation of well logging data, i.e. for porosity (PHI), shaliness (VCL) and water saturation in the uninvaded zone (SW) (Fig. 4). As seen in the porosity histogram, samples with porosity ranging from 0 to 26% were uniformly distributed

Table 1

Stratigraphy of the Sędziszów 34 borehole

Depth interval [m]	Stratigraphy
0–20	Quaternary
20–135	Miocene of Rzeszów Bay
135–833	Neogene Stebnik Unit
833–996	allochthonous Miocene
996–2928	autochthonous Miocene – Sarmatian + Upper Badenian
2928–2950	autochthonous Miocene – Middle Badenian
2950–2953	autochthonous Miocene – Lower Badenian
2953–3000	Lower Carboniferous – Visean

Table 2

Logs and results of the comprehensive interpretation of the Sędziszów 34 borehole, in the depth section 1300–2931 m

No	Symbol	Unit	Parameter	Log
1	DT	μs/m	transit interval time	Sonic, PA
2	GR	API	intensity of natural radioactivity	Gamma Ray, PG
	GRC	API	intensity of natural radioactivity without uranium window	Spectral Gamma Ray, sPG
3	HO01, HO06, HO09, HO12	ohmm	apparent resistivity recorded in various distances from borehole axis	Resistivity, HRAI
4	RTH, RXH0	ohmm	true resistivity of uninvaded zone and flushed zone	Resistivity, HRAI
5	RHOB	g/cm^3	bulk density	Density, PGG
6	VP, VS, VST	km/s	velocity of P-wave, S-wave and Stoneley wave, respectively from acoustic full waveforms	Sonic, FWS
7	RAT		velocity ratio, VP/VS	Sonic, FWS
8	NI		Poisson ratio	Sonic, FWS
9	K, E	GPa	bulk modulus, Young modulus, respectively	Sonic, FWS
10	PHI	%	total porosity	comprehensive interpretation
11	SW, SX0	%	water saturation in uninvaded zone	comprehensive interpretation
12	VSA, VCL	%	volume of sandstone and shaliness, respectively	comprehensive interpretation

and the plot was similar in shape to a Gaussian graph. A greater number of data points in the first three classes showed that shaliness has strong effect on petrophysical parameters. A slightly greater sample size in the 63.8–73.6% classes was a result of greater gamma ray log anomalies within the natural radioactivity range shown in Figure 3. Histogram SW, skewed as compared to a Gaussian graph, further indicated that there was high water saturation levels in the rocks. This was also seen in the greatest sample size in the last class in Figure 4.

Frequency histograms of the VP, VS and VP/VS ratios were calculated based on results of automatic interpretation of acoustic waveforms recorded with the Full Wave Sonic (FWS) device (Jarzyna et al., 2007). Distributions of velocities and the velocity ratio were almost normal (Fig. 6). This means that all geological factors such as mineral composition (including shaliness), porosity, and water- or gas-saturation equally affected P-wave and S-wave velocity within the Sarmatian succession. The normal distribution in the RAT histogram showed no distinct anomalies in plots of VP vs. depth and VS vs. depth.

Histograms of elastic moduli K and NI (Fig. 7) that were child values of VP and VS and RHOB were also computed. As expected, the histograms approximated to normal distributions.

Moreover, basic statistics were calculated for all parameters (Table 3). Variance ranges of the parameters could be traced. The same values of the mean and median values were consistent with the normal distributions seen in analysis of the histograms. Standard deviations in comparison to average values illustrated the level of credibility of parameters determined.

FRACTAL CORRELATION DIMENSION

The fractal correlation dimension D_2 is a generalized dimension of the second order calculated on the basis of the correlation integral $C(r)$. D_2 was calculated with the use of *Wymiar* software (Harasim, 2003) from the slope of a linear section of a plot of $C(r)$ vs. r in a double logarithmic scale:

$$D_2 = \lim_{r \to 0} \frac{\log C(r)}{\log r} \quad [1]$$

$$C(r) = \lim_{r \to 0} \left[\frac{1}{N^2} \sum_{i,j=1}^{N} H(r - |x_i - x_j|) \right] \quad [2]$$

where: $C(r)$ – correlation integral, N – number of data, $H(z)$ – Heaviside's unit step function: $H(z) = \begin{cases} 0 \ldots\ldots z \le 0 \\ 1 \ldots\ldots z < 0 \end{cases}$ (Bracewell, 2000), x_i, x_j – coordinates of the data measured, r – distance (Grassberger and Procaccia, 1983).

Calculations were made for a data set in which parameters acquired from well logging were a function of depth; hence, the variability of fractal dimension was analysed as a function of depth with a depth step equal to 0.1 m. The depth window for D_2 calculations was selected to have 50 points (5 m), and the calculation window was being shifted by one measurement point with depth. The calculated value, D_2, was assigned to the centre of the calculation window. As a result we obtained sets of correlation dimensions, D_2, for logging parameters as a function of depth. Since the fractal correlation dimension depended on the number of samples, the window width was so chosen that the number of samples was minimal enough to obtain reliable calculations for the fractal dimensions. Also, the window was shifted with a specially chosen step so as to be able to see fractal dimension changes with depth. Choosing too big a step resulted in overlooking the change, particularly when the thickness of the Sarmatian rocks varied markedly.

The shape of the fractal dimension, D_2, vs. depth for apparent resistivity measured with the HRAI tool with minimum (HO01) and maximum (HO12) radial distance at a depth interval of 1300–2980 m of the autochthonous Miocene deposits

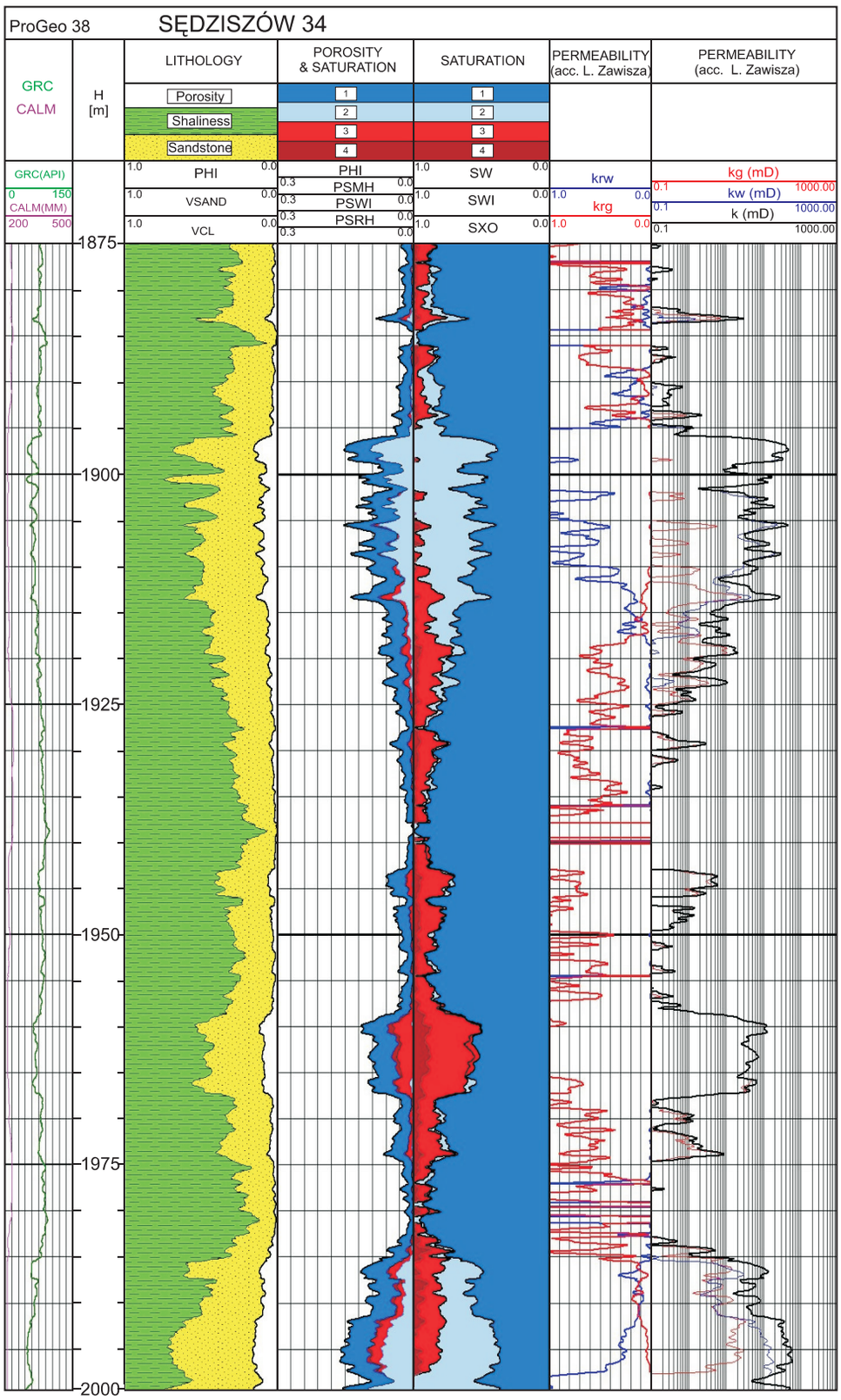

Fig. 2. Results of the comprehensive interpretation of well logging for the 1875–2000 m interval (PGNiG Warsaw, Branch in Sanok, Jasło Office, 2009)

PHI – porosity, VSAND – volume of sandstone, VCL – volume of clay minerals; 1 – bound water, 2 – free water, 3 – movable hydrocarbons, 4 – residual hydrocarbons, PSMH – part of rock occupied by movable hydrocarbons, PSWI – part of rock occupied by irreducible water, PSRH – part of rock occupied by residual hydrocarbons, SW – water saturation, SWI – irreducible water saturation, SXO – water saturation in flushed zone, krw – relative permeability of water, krg – relative permeability of gas, kg – phase gas permeability, kw – phase water permeability, k – absolute permeability; depth of gas inflow (1959–1966 m) is marked with a brown bar

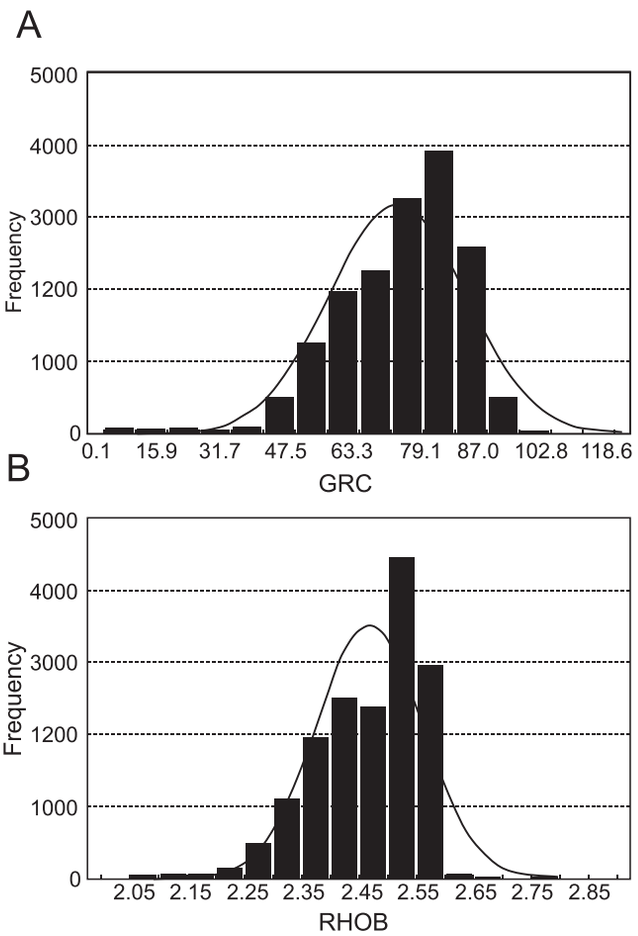

Fig. 3. Frequency histograms of:
A – natural gamma radioactivity (GRC), B – bulk density (RHOB)

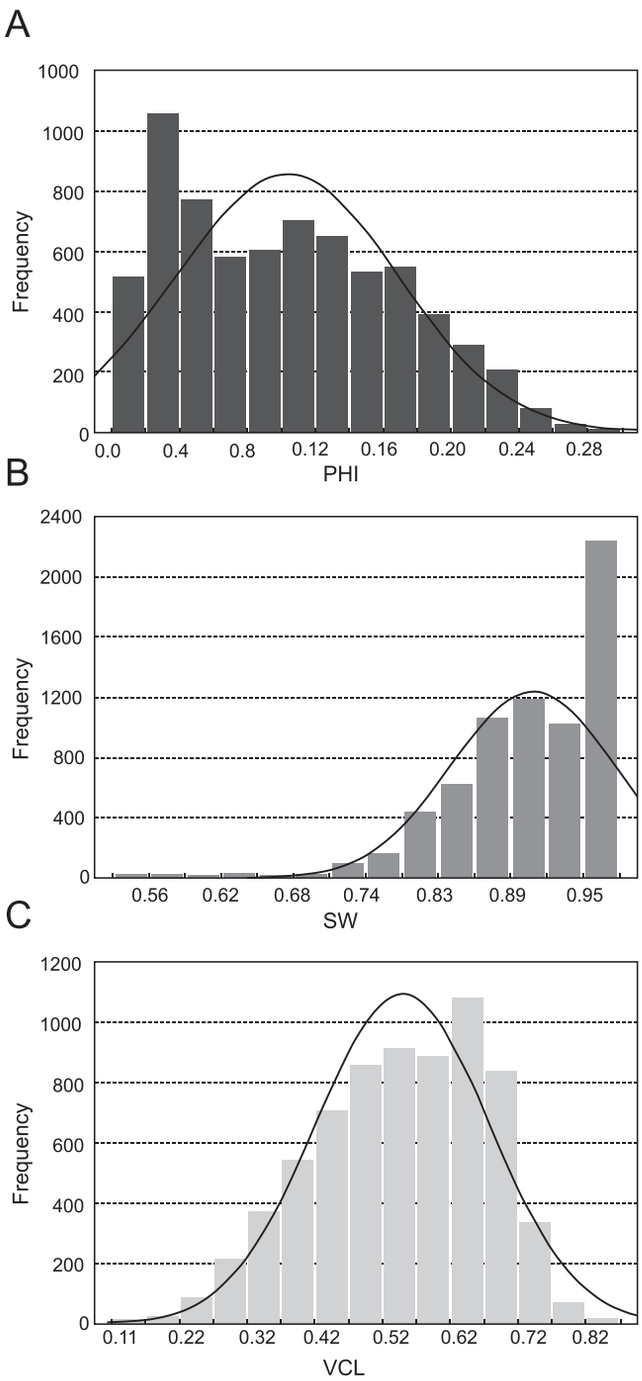

Fig. 4. Frequency histograms of: A – porosity (PHI), B – water saturation in the uninvaded zone (SW), C – shaliness (VCL)

mirrored the shape of the lithology curves (Fig. 8). In the first path there were GRC curves, a result of gamma ray logging including thorium and potassium content, and the fractal dimension for this log, D_2GRC. In the upper part of the plot one could observe separate courses of GRC and D_2GRC for sandstones with distinct porosity. The GRC curve had low and rather stable values of natural radioactivity while the D_2GR values were more variable with increased values from thin sandstone beds. In the lower part of the plot, where deposits with distinct shaliness dominated, GRC and D_2GRC were almost parallel. The caliper log for this part of the plot did not reveal significant variations except for a bed at a depth of 2720–2800 m. However, this anomaly did not correlate with any other changes. A group of anomalies corresponding to sequences of sandstones and shales at the lithology solution could be observed in the D_2 curves for the resistivity logs HO01 and HO12. Similar features were observed in the bulk density curve and the fractal dimension for RHOB.

In all plots, amplitudes of the D_2 anomaly were not as large as anomaly amplitudes in resistivity and bulk density logs. One could observe clear resistivity variations, which correlated with the changes of sandstone volume, but there was no similarity between the D_2 of the resistivity curves and the resistivity curves. A similar trend could be observed in variations of RHOB and D_2RH curves. This was valid only to a depth of 2160 m and below that there were clear variations in D_2RH but no changes in RHOB. Figure 8 also shows the filtered logs (FHO01 and FHO12) and filtered fractal dimensions (FD_2HO01, FD_2HO12 and FD_2RH). A filter as the running 9 point average (0.90 m) was used. There were observed similar tendencies in RHOB and D_2RH while trends of changes in the resistivity logs and their fractal dimension were not the same.

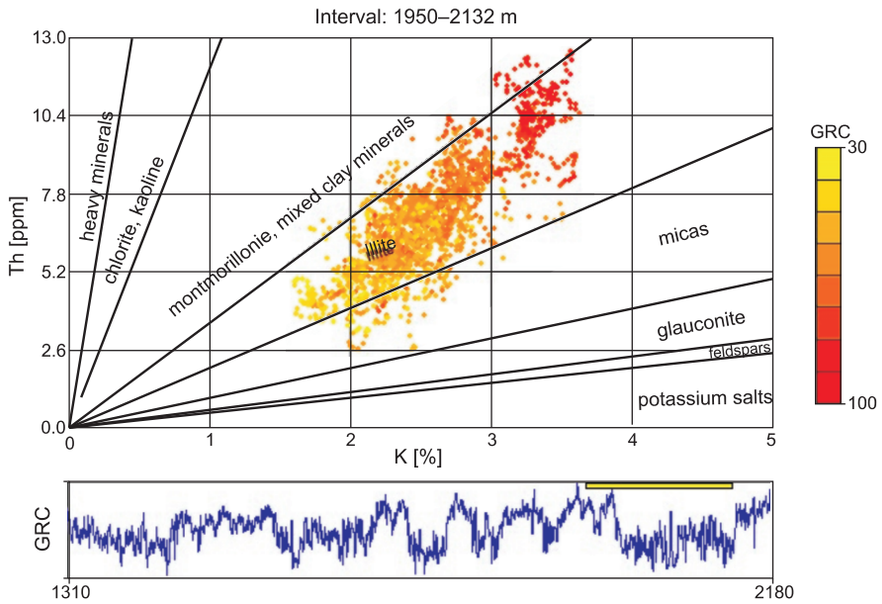

Fig. 5. Cross-plot of thorium vs. potassium in the Sędziszów 34 borehole in the depth section of 1950–2132 m

Sandstone dominated in that part of the geological profile

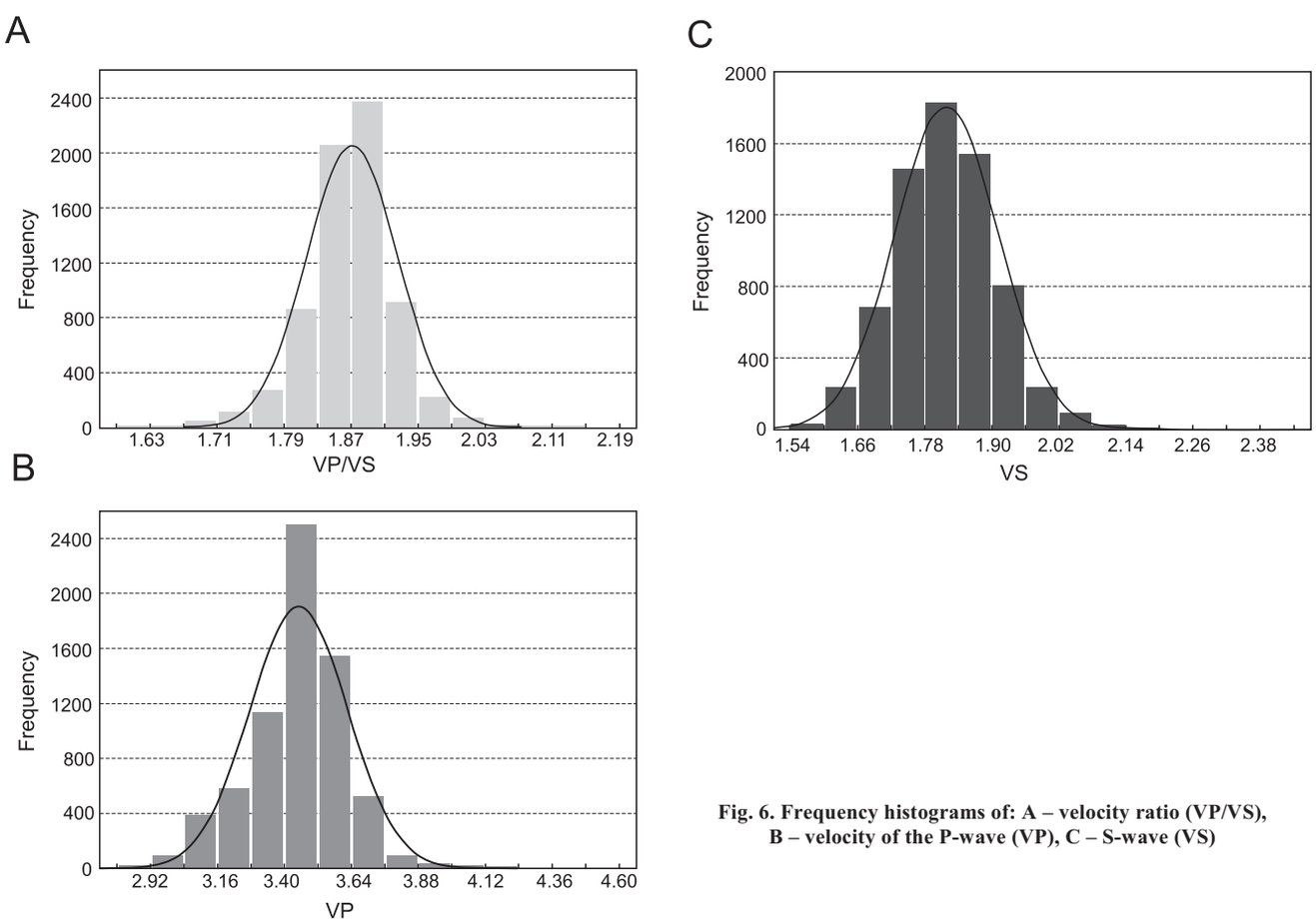

Fig. 6. Frequency histograms of: A – velocity ratio (VP/VS), B – velocity of the P-wave (VP), C – S-wave (VS)

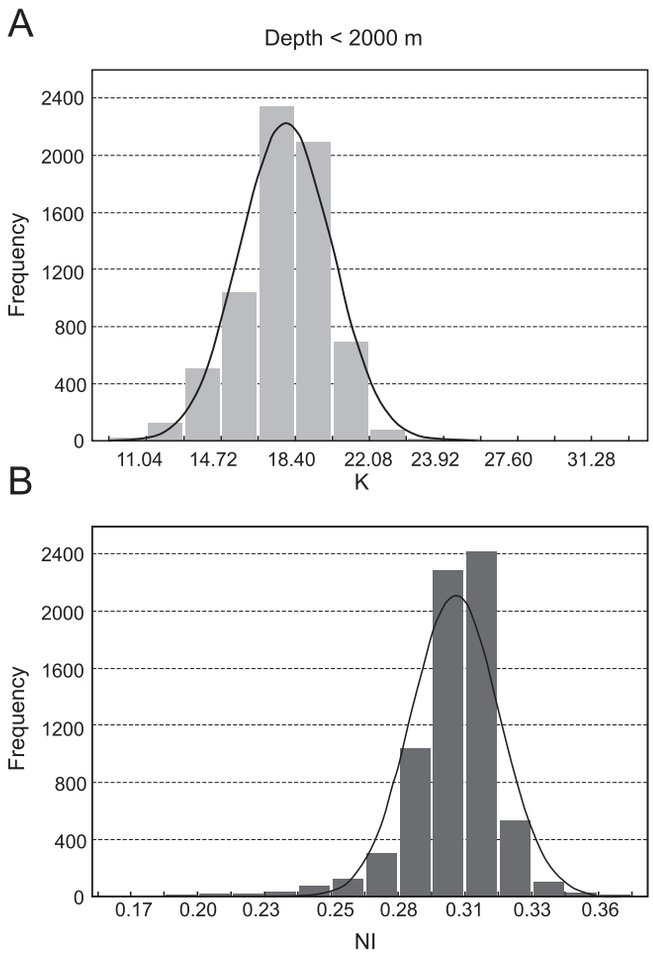

Fig. 7. Histograms of: A – bulk modulus (K), B – Poisson coefficient (NI)

Values of D_2HO01 ranged from 0.67 to 0.99, with a mean value of 0.86 for HO01 m. Values of D_2H012 varied from 0.66 to 0.97, with the same mean value as in the previous case. Basic statistics for the fractal dimension were the same. However, one can observe different values of D_2 depending on the lithology. Variations of D_2HO01 and D_2HO12 values may signal heterogeneity of the rock formation in the flushed zone. The scatter diagram for HO01 vs. HO12 pointed to heterogeneities (Fig. 9).

The linear regression equations calculated for the chosen parameters are shown in Table 4. High correlation coefficients between apparent resistivity in zones at different distances from the borehole wall were observed. One could also see that there was strong correlation between some fractal dimensions, e.g., D_2HO09 vs. D_2HO12, D_2HO06 vs. D_2HO09 and D_2HO06 vs. D_2HO12, and poorer correlation between D_2H001 vs. D_2H012 or D_2H001 vs. D_2HO09. However, the parameters and their fractal dimensions did not correlate.

High values of correlation coefficients for fractal dimensions D_2 for apparent resistivity in zones with great radial distances showed that there was fractal similarity of the end parts of the invaded zone. No similarity could be observed in the flushed zone, which was characterized by D_2HO01, and the invaded zone by D_2HO06. This could be explained by filtration

Table 3

Basic statistics calculated for selected parameters in the depth section 1300–2928 m (Sarmatian and Upper Badenian deposits)

Parameter	Average	Min	Max	Standard deviation
GRC [API]	73	33	125	14
DT [μ/m]	288	218	380	17
RHOB [g/cc]	2.48	1.91	2.71	0.09
HO01 [ohmm]	1.70	0.58	6.18	0.56
HO06 [ohmm]	1.75	0.57	6.13	0.61
HO09 [ohmm]	1.75	0.57	6.08	0.61
HO12 [ohmm]	1.76	0.57	6.09	0.62
PHI	0.07	0.00	0.25	0.05
SW	0.91	0.49	1.00	0.08
VSA	0.37	0.00	0.87	0.11
VCL	0.57	0.05	1.00	0.15
VP [km/s]	3.57	2.80	4.58	0.21
VS [km/s]	1.89	1.54	2.52	0.12
VST [km/s]	1.37	1.20	1.78	0.05
RAT	1.89	1.56	2.26	0.06
E [MPa]	23	14	40	3.11
K [MPa]	20	9.21	37.09	2.96
NI	0.31	0.15	0.38	0.02

penetrating into the porous and permeable rock formation, and as a result of rock resistivity changing at different distances from the borehole axis. The results obtained helped infer as to on how deep the invaded zone extended: up to HO06 penetration depth.

Mean values of the fractal dimension D_2 for resistivity measured by the short device (HO01) and long device (HO12), and bulk density (RHOB) are given to shown that changes in fractal dimension related to type of lithology and type of media saturating pore space were helpful in distinguishing between various types of beds (Table 5).

The relationship between elastic parameters and their fractal dimensions was also studied. Histograms of fractal dimensions D_2 were calculated for VP, VS, and RAT (Fig. 10). The shape of all histograms was similar to the shape of the normal distribution curve, with the left branch elongated. Fractal dimensions D_2 for velocity had large values oscillating around 0.83, and only locally they dropped below 0.65. The large values gave evidence that the depth distribution of the parameters studied was uniform (Kotuła et al., 2001). A similar conclusion could be drawn from the D_2NI histogram (Fig. 11). However, the shape of the D_2K histogram was influenced by velocity variations and bulk density changes.

The variability of the fractal dimension for VP (D_2VP) and VS (D_2VS) and velocity ratio (D_2VP/VS) with depth was also studied (Fig. 12). For a depth interval of 1400–1430 m, the curves were almost parallel. Water saturation fluctuated between 80 and 100%. For the 1957–1962 m interval, where there was a significant inflow of gas, the fractal dimension D_2VP dropped while D_2VS rose. To illustrate this relationship, regression equations and correlation coefficients are shown for the velocities VP, VS, VP/VS, and their fractal dimensions

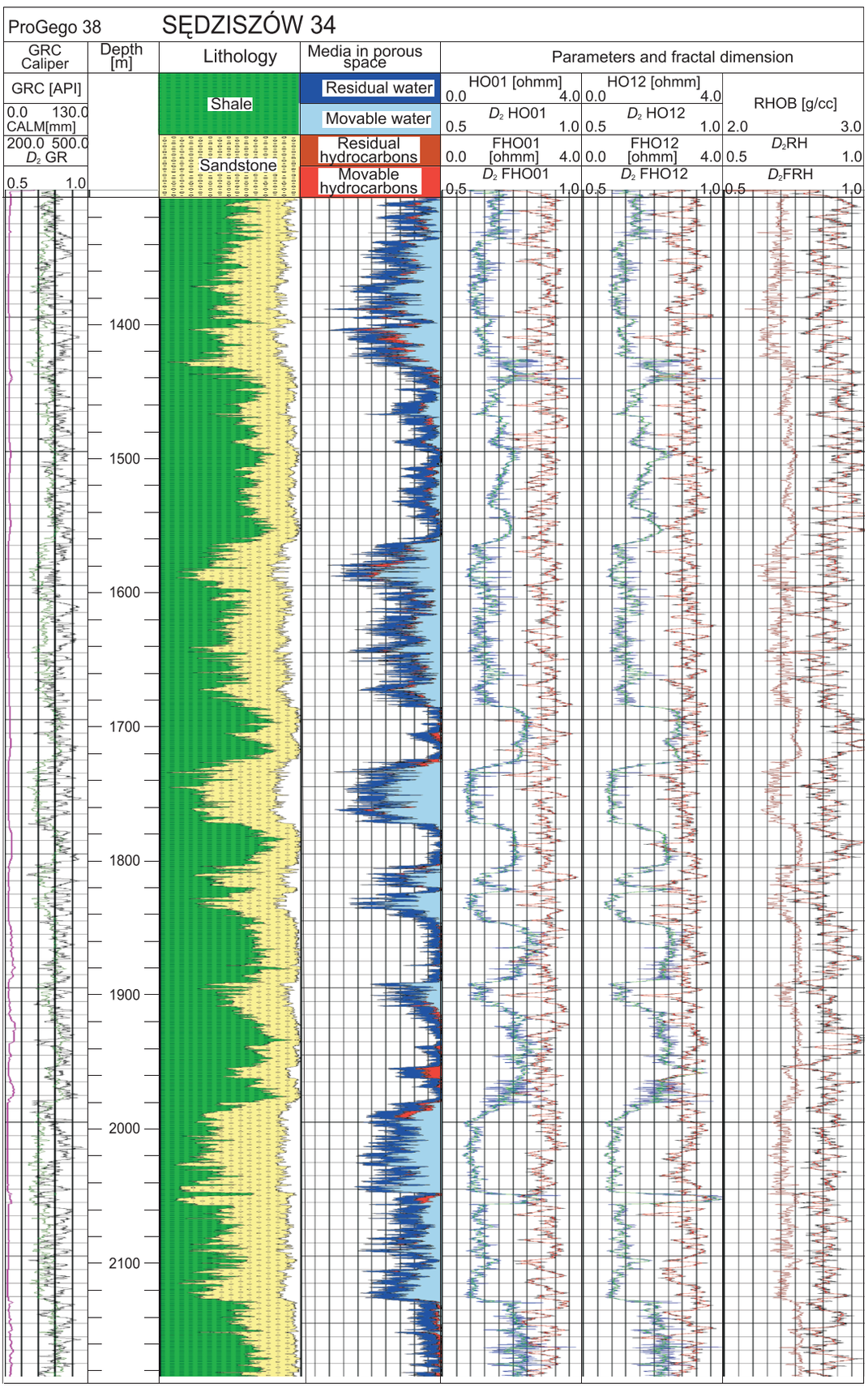

Fig. 8. Parameters and fractal dimension D_2 for results of gamma ray log (GRC) two-resistivity from high resolution array induction log, HRAI – resistivity log (HO01 and HO12) and lithology–porosity–saturation solution for the depth interval 1300–2980 m

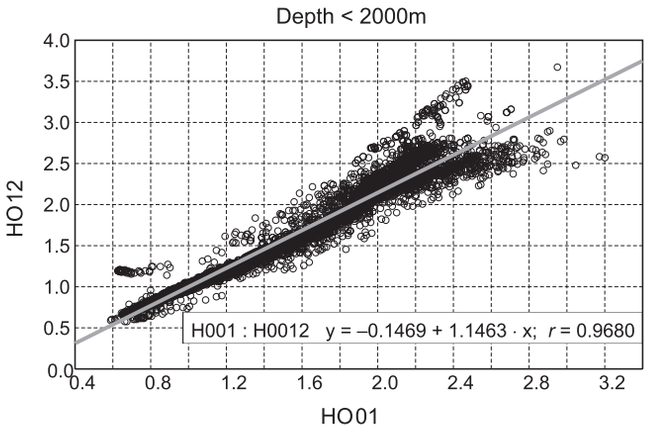

Fig. 9. Scatter plot for apparent resistivity measured with the HRAI tool

HO012 – resistivity of zone with radial distance 120";
HO01 – resistivity of flushed zone, radial distance 10"

Table 4

Regression equations and correlation coefficients for apparent resistivity recorded with HRAI and their fractal dimensions

Parameters	Equation	Correlation coefficient
HO01 vs. HO012	y = –0.1469 + 1.1463 · x	r = 0.97
HO01 vs. HO06	y = –0.1177 + 1.119 · x	r = 0.97
HO01 vs. HO09	y = –0.1393 + 1.1393 · x	r = 0.97
D_2HO06 vs. D_2HO12	y = 0.0965 + 0.8894 · x	r = 0.92
D_2HO06 vs. D_2HO09	y = 0.0924 + 0.8937 · x	r = 0.93
D_2HO09 vs. D_2HO12	y = 0.019 + 0.9785 · x	r = 0.97
D_2HO01 vs. D_2HO12	y = 0.4865 + 0.4382 · x	r = 0.44

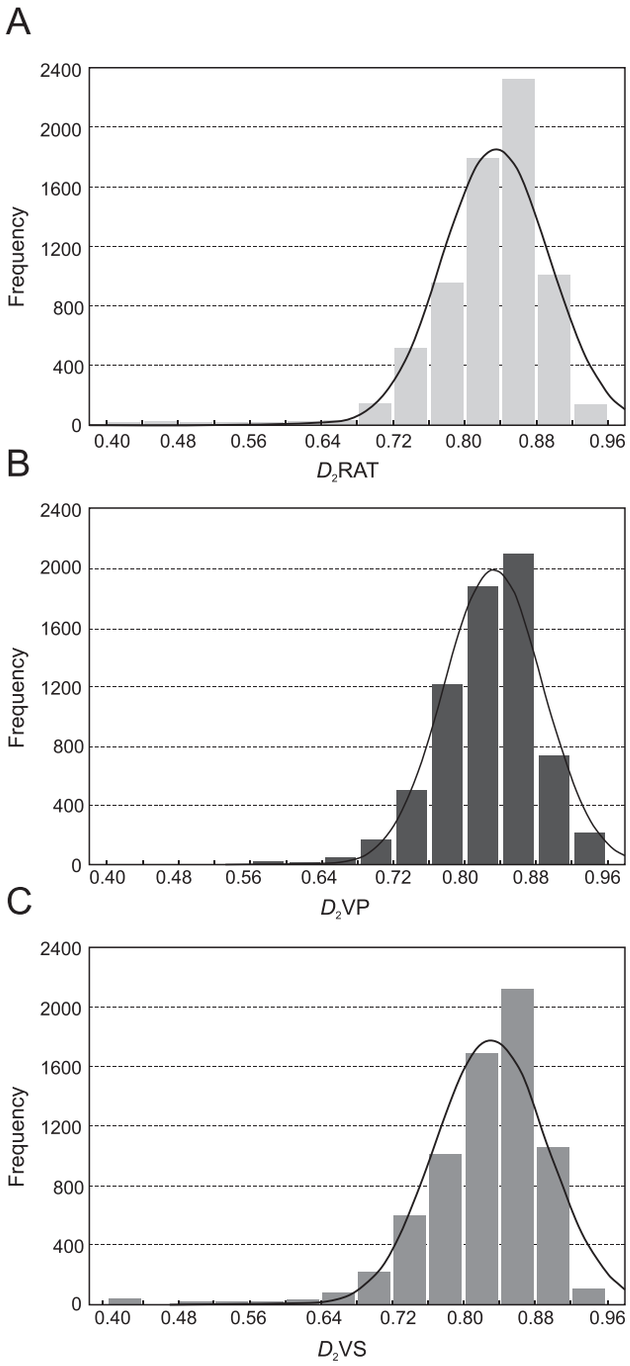

Fig. 10. Frequency histograms of the fractal dimensions: A – D_2RAT, B – D_2VP, C – D_2VS

Table 5

Mean values of the fractal dimension D_2 for HO01 resistivity, HO12 resistivity and bulk density, RHOB

Depth interval [m]	Mean value			Lithology
	D_2HO01	D_2HO12	D_2RH	
1410–1440	0.8795	0.8727	0.8756	gas-saturated sandstones
1570–1605	0.8723	0.8636	0.8636	gas-saturated sandstones
1730–1770	0.8571	0.8434	0.8611	water-saturated sandstones with gas traces
1990–2038	0.8687	0.8636	0.8620	water-saturated sandstones with gas at the top
2110–2132	0.8808	0.8879	0.8650	water-saturated sandstones
2457.5–2480	0.8316	0.8726	0.8347	sandy shales

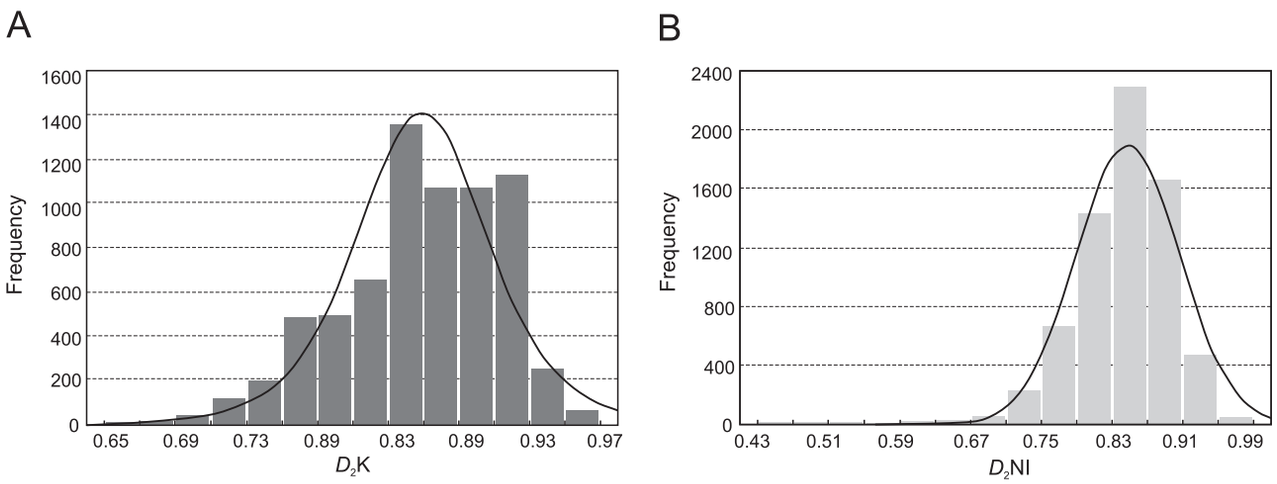

Fig. 11. Frequency histograms of fractal dimension: A – D_2K (bulk modulus), B – D_2NI (Poisson coefficient)

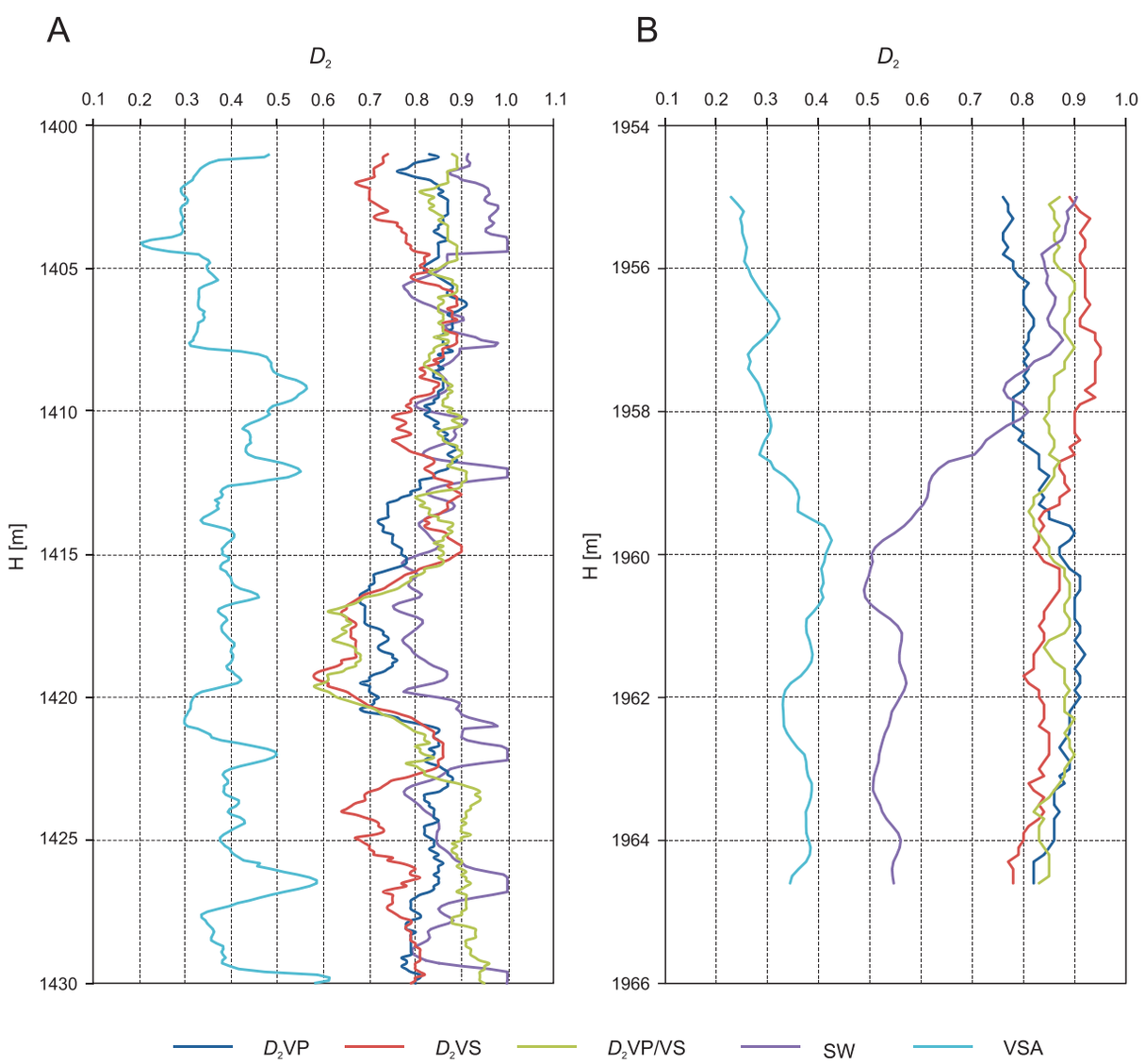

Fig. 12. Fractal dimensions for VP, VS, and VP/VS ratio vs. depth (H) in the intervals: A – 1400–1430 m, B – 1955–1968 m (high gas saturation); water saturation (SW) and sandstone volume (VSA) are also shown

(Table 6). The regression was made over the whole study interval and for a depth section of 1950–1980 m where there were sandstone beds with increased gas saturation. The correlation included also Stoneley waves (VST) and porosity PHI obtained from comprehensive interpretation of the well logs. The correlation between velocities was high for both depth intervals. There was no correlation between velocity and its fractal dimension. The same relation could be observed for porosity PHI and its fractal dimension D_2PHI.

The relationship between longitudinal wave velocity (VP) and fractal dimension (D_2VP) was also studied in the depth section 1900–2000 m. Categories were defined with respect to the VP/VS ratio. The first group included points that corresponded to beds saturated with gas, for which VP/VS < 1.59. VP/VS ratio increased with increasing shaliness of rock, up tu 2.3 for claystones. Correlation coefficients in all categories were not high. Only in the first class, with low VP/VS, the coefficient was high, thought due to the small number of samples this result can be neglected. Thus, in the case of sandstone–mudston–shale rocks, the fractal dimension related to the VP/VS category was of importance in identification of gas-saturated rocks alone. The result was of no use to evaluate rock shaliness.

The study included also relationships between results of the comprehensive interpretation: porosity (PHI), water saturation in flushed zone (SWXO) and uninvaded zone (SW), shaliness (VCL) and sandstone volume (VSA), and their fractal dimensions D_2. Examples of the relationships: VCL vs. PHI and their

Table 6

Regression equations and linear correlation coefficients for VP, VS, VP/VS, and their fractal dimensions

Parameters	Equation	Correlation oefficient
VP vs.VS	y = 0.2374 + 0.4628 · x	r = 0.82, full interval
VP vs. D_2VP	y = 0.6956 + 0.0393 · x	r = 0.12, full interval
VP vs. VS	y = 0.188 + 0.4779 · x	r = 0.86; depth section 1950–1980 m
VP vs. D_2VP	y = 0.6989 + 0.0397 · x	r = 0.17; depth section 1950–1980 m
VP vs. VST	y = 0.7547 + 0.1722 · x	r = 0.75; depth section 1950–1980 m
PHI vs. D_2VP	y = 0.8535 – 0.1892 · x	r = –0.19; depth section 1950–1980 m

fractal dimensions D_2VCL vs. D_2PHI as well as VSA vs. VCL and D_2VSA vs. D_2VCL for a depth of 1950–1970 m are shown in Figure 13. Fractal dimensions had much lower correlation coefficients, though one could see a clear variability trend, which was opposite to that for the basic parameters. Similar coefficient values for correlation between parameters and their fractal dimensions could be observed for other intervals.

A scatter plot VCL vs. PHI for five selected classes of water saturation for the depth interval 1855–1870 m was analysed

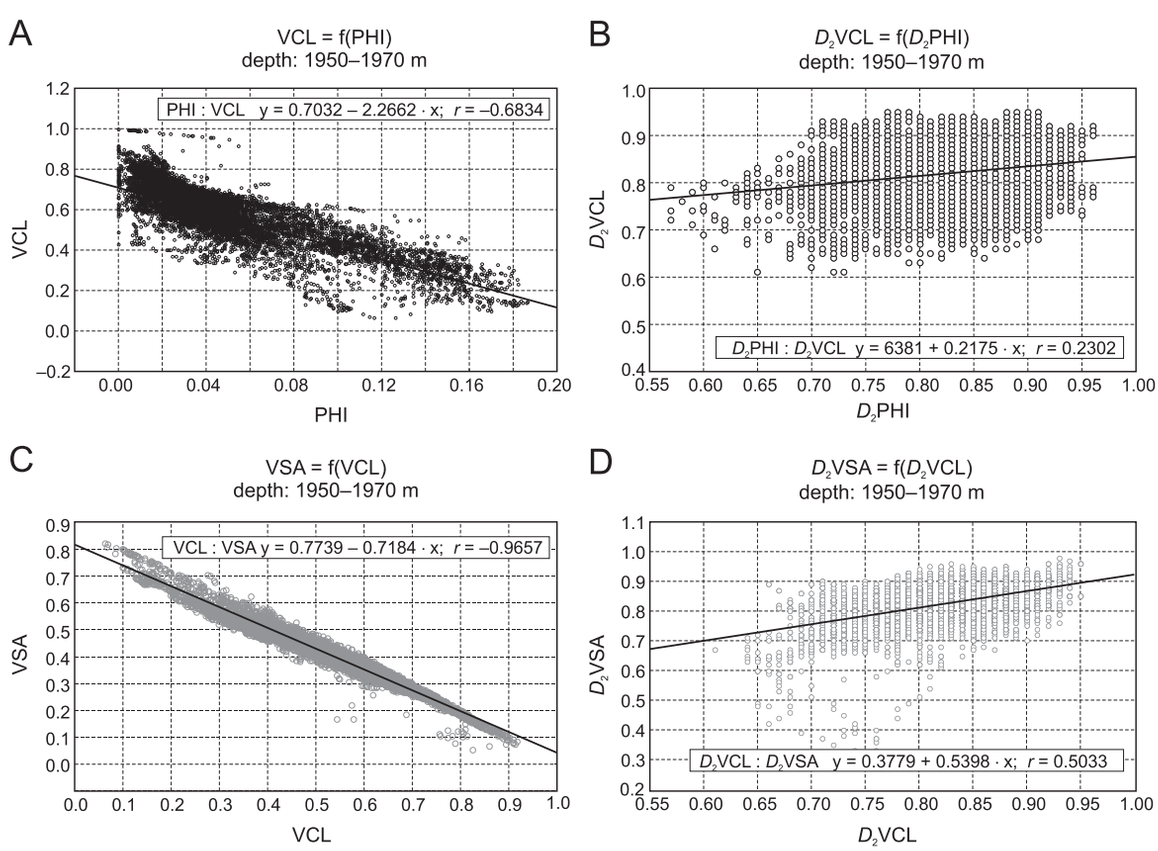

Fig. 13. Relationships between VCL and PHI (A) and fractal dimensions D_2VCL and D_2PHI (B) and between VSA and VCL (C) and D_2VSA and D_2VCL (D)

(Fig. 14). In all classes, the regression line had a similar slope and points in successive plots represented the number of layers with gas saturation at different levels. Table 7 shows correlation parameters for these relationships.

High correlation coefficients for five selected classes of SW showed that there was close dependence between VCL and PHI. The lowest correlation coefficients were observed for rocks with the highest gas saturation. It was assumed that those were rocks in which gas was supposed to occur not only in porous sandstones (high PHI) but also in rocks with high shaliness (high VCL). Rocks with the greatest water saturation had higher correlation coefficients between PHI and VCL.

Likewise, the dependence between bulk density and interval transit time for the P-wave was studied. The analysis included only Sarmatian rocks. Five groups of porosity PHI were distinguished over the range of 0–0.25. Scatter plots of RHOB vs. DT were analysed (Fig. 15) and the expected dependence was shown. Points with low bulk density and high interval transit times showed that there was evident residual gas saturation in the flushed zone.

High correlation coefficients indicated that there were important relationships between variables (Table 8). The slopes of regression lines in four classes were much alike and this showed the similar character of relationships and similar factors that affect bulk density and transit interval time. A higher slope of the regression line in the first class pointed to the fact that selected bulk densities corresponded to higher specific transit interval times and hence, there was a clear influence of the density of the mineral framework.

Table 7

Regression equations PHI vs.VCL for five selected classes of water saturation in the uninvaded zone

Saturation class	Equation	Correlation coefficient
SW: (0.5, 0.6)	y = 0.7093 – 2.2012 · x	r = –0.50
SW: (0.6, 0.7)	y = 0.6134 – 1.6649 · x	r = –0.37
SW: (0.7, 0.8)	y = 0.6477 – 1.748 · x	r = –0.54
SW: (0.8, 0.9)	y = 0.6935 – 1.8931 · x	r = –0.73
SW: (0.9, 1.0)	y = 0.7099 – 2.4133 · x	r = –0.68

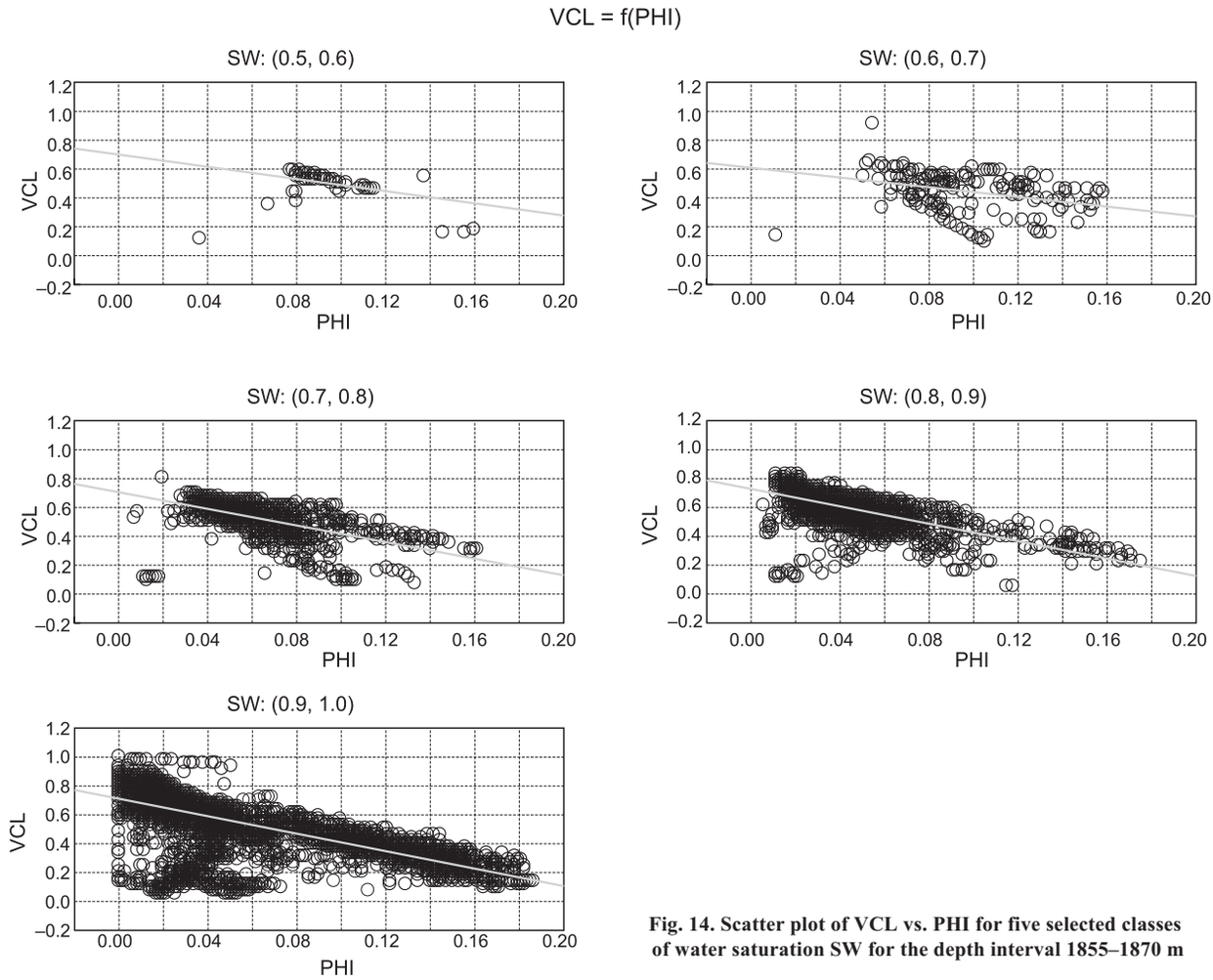

Fig. 14. Scatter plot of VCL vs. PHI for five selected classes of water saturation SW for the depth interval 1855–1870 m

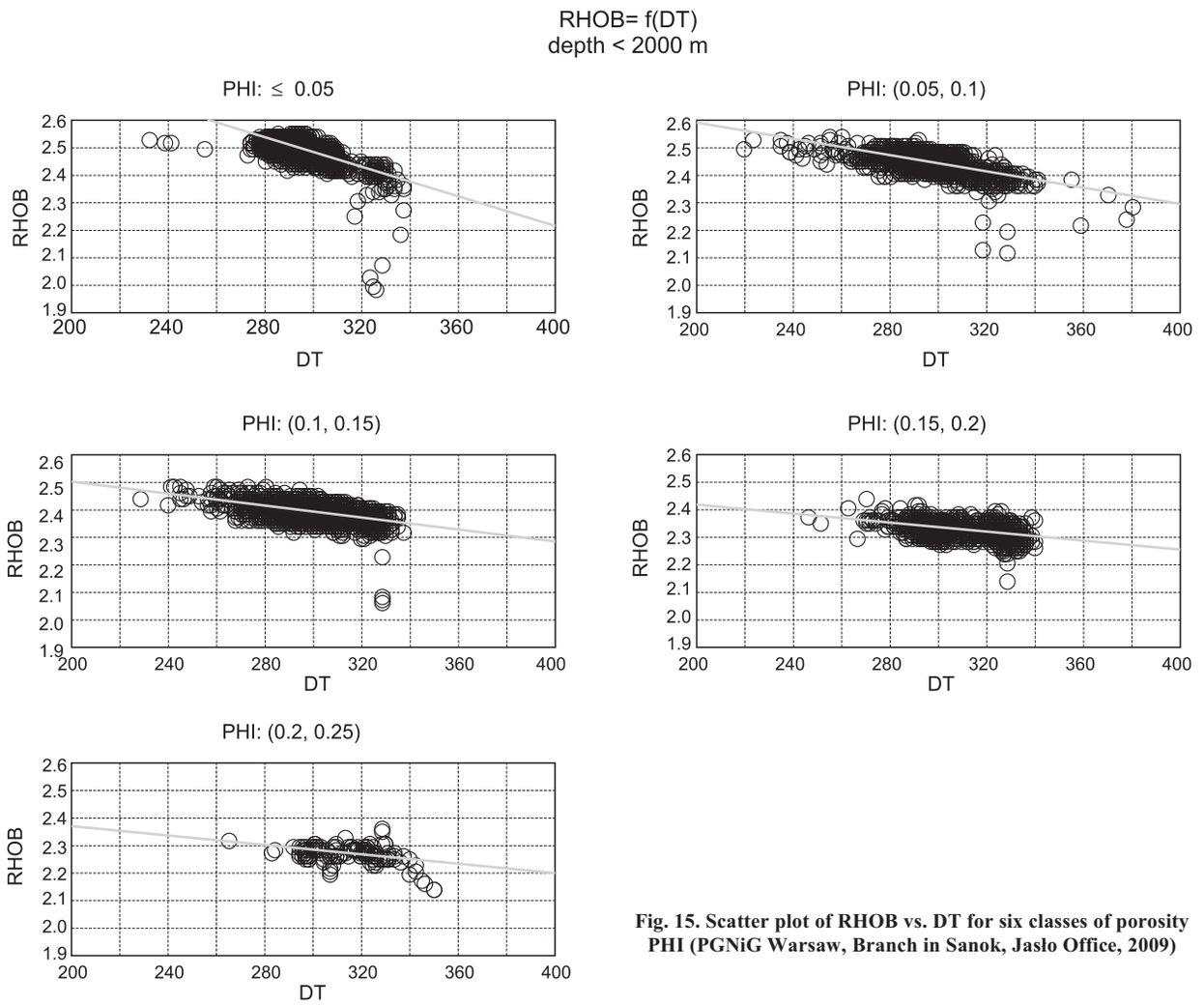

Fig. 15. Scatter plot of RHOB vs. DT for six classes of porosity PHI (PGNiG Warsaw, Branch in Sanok, Jasło Office, 2009)

Table 8

Regression equations RHOB vs. DT for five selected classes of porosity

Porosity class	Equation	Correlation coefficient
PHI: (0.00, 0.05)	y = 3.2915 – 0.0027 · x	r = –0.70
PHI: (0.05, 0.10)	y = 2.8877 – 0.0015 · x	r = –0.63
PHI: (0.10, 0.15)	y = 2.7207 – 0.0011 · x	r = –0.54
PHI: (0.15, 0.20)	y = 2.5826 – 0.0008 · x	r = –0.44
PHI: (0.20, 0.25)	y = 2.541 – 0.0009 · x	r = –0.40

SUMMARY

It maybe seen that statistical analyses – and fractal analysis in particular – provide a good approach to studying thin-bedded sandstone-shale rocks of the Carpathian Foredeep. Frequency histograms of parameters measured by well logging and results of the comprehensive interpretation of well logs, i.e. porosity and water- and gas-saturation maybe useful in evaluating variability in the physical properties of rocks.

Incorporating fractal analysis to variability evaluation gives a broader look at the variability of shaly reservoir rocks. The good correlation of fractal dimensions among themselves and between selected petrophysical parameters showed that the curves analysed, which represent parameters important to the evaluation of rock properties, have the same type of complexity. The correlation coefficient was calculated for the assumed confidence interval, p > 05, and showed pairs of fractal dimensions for those parameters which have similar variability and the same complexity (curve smoothness or curve roughness).

The study showed that not all parameters correlated with their fractal dimensions. A change in the fractal dimension did not need to correlate with a change in the given parameter as the correlation dimension (D_2) describes the "type" of complexity of the parameter (curve roughness). The variability of parameters and their fractal dimensions may indicate complexity of the pore structure and how shaliness influences the reservoir properties of the Miocene strata. Therefore, the results have practical benefits, giving extra information on thin-bedded reservoir rock formations.

Acknowledgments. The results presented were obtained during realization of project nr N N525 363537 at the AGH University of Science and Technology, Kraków, Poland, Faculty of Geology Geophysics and Environmental Protection, financially supported by the Ministry of Science and Higher Education in Poland, 2009–2012. The authors thank POGC, Warsaw, Poland for making the data available for research.

REFERENCES

ÁLVAREZ G., SANSÓ B., MICHELENA R.J. and JIMÉNEZ J.R. (2003) – Lithologic characterization of a reservoir using continuous-wavelet transforms. IEEE Transactions on Geosciences and Remote Sensing, **41** (1): 59–65.

BAŁA M. (2011) – Evaluation of electric parameters of anisotropic sandy-shaly Miocene formations on the basis of resistivity logs. Acta Geophys., **59** (5): 954–966.

BORYS Z. and MYŚLIWIEC M. (2002) – The prospectivity prognosis of the hydrocarbon discoveries in the Carpathians and the Carpathian Foredeep (in Polish with English summary). Nafta-Gaz, **9**: 447–455.

BORYS Z., MYŚLIWIEC M. and TRYGAR H. (2000) – New gas discoveries in the Carpathian Foredeep, Poland, as the result of the seismic anomalies interpretation. Oil and Gas News from Poland, **10**: 69–80.

BRACEWELL R. (2000) – The Fourier Transform and its applications, 3rd ed. New York: McGraw-Hill: 61–65.

DOCUMENTATION of the Sędziszów 34 borehole (2009) – Archiwum PGNiG S.A., Oddział w Sanoku, Biuro w Jaśle (in Polish). Arch. PGNiG Warsaw, Branch in Sanok, Jasło Office.

GRASSBERGER P. and PROCACCIA I. (1983) – Measuring the strangeness of strange attractors. Physica 9D: 189–208.

HARASIM M. (2003) – Analiza metod szacowania wybranych parametrów dynamiki nieliniowej na przykładzie danych lokalnej sejsmiczności górniczej. M.Sc. thesis, Library of Faculty of Geology Geophysics and Environmental Protection, AGH UST, Kraków, Poland.

JARZYNA J., BAŁA M., CICHY A., GĄDEK W., GĄSIOR I., KARCZEWSKI J., MARZENCKI K., STADTMÜLLER M., TWARÓG W. and ZORSKI T. (2007) – Przetwarzanie i interpretacja profilowań geofizyki wiertniczej, system GeoWin (ed. J. Jarzyna). Arbor, Kraków.

KARNKOWSKI P. (1994) – Miocene deposits of the Carpathian Foredeep (according to results of oil and gas prospecting). Geol. Quart., **38** (3): 377–394.

KARNKOWSKI P. (1999) – Oil and gas deposits in Poland. Geosynoptics Society "Geos", Kraków.

KOTARBA M.J., PERYT T.M. and KOLTUN Y.V. (2011) – Microbial gas system and prospectives of hydrocarbon exploration in Miocene strata of the Polish and Ukrainian Carpathian Foredeep. Ann. Soc. Geol. Pol., **81** (3): 523–544.

KOTUŁA M., JARZYNA J. and MORTIMER Z. (2001) – Badanie wymiaru fraktalnego parametrów petrofizycznych. In: Nauki o Ziemi w badaniach podstawowych, złożowych i ochronie środowiska na progu XXI wieku. WGGiO, Kraków: 107–111.

KRZYWIEC P., ALEKSANDROWSKI P., RYZNER-SIUPIK B., PAPIERNIK B., SIUPIK J., MASTALERZ K., WYSOCKA A. and KASINSKI J. (2005) – Geological structure and origin of the Miocene Ryszkowa Wola Horst (Sieniawa–Rudka area, eastern part of the Carpathian Foredeep Basin) – results of 3D seismic data interpretation (in Polish with English summary). Prz. Geol., **53** (8): 656–663.

KRZYWIEC P., WYSOCKA A., OSZCZYPKO N., MASTALERZ K., PAPIERNIK B., WRÓBEL G., OSZCZYPKO-CLOVES M., ALEKSANDROWSKI P., MADEJ K. and KIJEWSKA S. (2008) – Evolution of the Miocene deposits of the Carpathian Foredeep in the vicinity of Rzeszów (the Sokołów–Smolarzyny 3D seismic survey area) (in Polish with English summary). Prz. Geol., **56** (4): 232–244.

LOPEZ M. and ALDANA M. (2007) – Facies recognition using wavelet based fractal analysis and waveform classifier at the Oritupano – a field, Venezuela, Nonlin. Proc. Geophys., **14**: 325–335, www.nonlin-processes-geophys.net/14/325/2007

MYŚLIWIEC M. (2004a) – Exploration for gas accumulations in the Miocene deposits of the Carpathian Foredeep using Direct Hydrocarbon Indicators (southern Poland) (in Polish with English summary). Prz. Geol., **52** (4): 299–306.

MYŚLIWIEC M. (2004b) – The Miocene reservoir rocks of the Carpathian Foredeep (in Polish with English summary). Prz. Geol., **52** (7): 581–592.

MYŚLIWIEC M. (2006) – Types of the Miocene reservoir rocks (Żołynia-Leżajsk gas field) and the methods of the gas reserves estimation (in Polish with English summary). Nafta-Gaz, **62** (4): 139–150.

MYŚLIWIEC M., PLEZIA B. and ŚWIĘTNICKA G. (2004a) – The Miocene gas fields discovered in the NE part of the Carpathian Foredeep on the base of the Direct Hydrocarbon Indicators on the seismic data. Prz. Geol., **52** (5): 395–402.

MYŚLIWIEC M., MADEJ K. and BYŚ I. (2004b) – The Miocene gas fields discovered in the Rzeszów area, Carpathian Foredeep, on the base of the Direct Hydrocarbon Indicators (in Polish with English summary). Prz. Geol., **52** (7): 501–506.

OSZCZYPKO N. (1998) – The Western Carpathian Foredeep – development of the foreland basin in front of the accretionary wedge and its burial history (Poland). Geol. Carpath., **49** (6): 415–431.

OSZCZYPKO N. and OSZCZYPKO-CLOWES M. (2012) – Stages of development in the Polish Carpathian Foredeep Basin. Cent. Eur. J. Geosc., **4**: 138–162.

OSZCZYPKO N., KRZYWIEC P., POPADYUK I. and PERYT T. (2006) – Carpathian Foredeep Basin (Poland and Ukraine): its sedimentary, structural, and geodynamic evolution. AAPG Mem., **84**: 293–350.

PAPE H., CLAUSER C. and IFFLAND J. (1999) – Permeability prediction based on fractal pore-space geometry. Geophysics, **64** (5): 1447–1460.

PIETSCH K., MARZEC P., KOBYLARSKI M., DANEK T., LEŚNIAK A., TATARATA A. and GRUSZCZYK E. (2007) – Identification of seismic anomalies caused by gas saturation on the basis of theoretical P and PS wavefield – Carpathian Foredeep, SE Poland. Acta Geophys., **55** (2): 191–205.

PORĘBSKI S. (1996) – Podstawy stratygrafii sekwencji w sukcesjach klastycznych. Prz. Geol., **44** (10): 995–1006.

SUCH P. (1998) – An application of fractal analysis in investigations of reservoir rocks. Abstract Book of the Conference and Exhibition. In: Modern Exploration and Improved Oil and Gas Recovery Methods. 1–4 September, Kraków.

SUCH P. (2004) – Analiza właściwości zbiornikowych i filtracyjnych rdzeni z otworów Chałupki Dębniańskie-3 i Jasionka-4. Materiały Konferencji Geopetrol, Zakopane 20–23.09.2004: 793–796.

ZORSKI T. (2009) – Recent improvements in interpretation methodology applied in GeoWin Satun application. Geologia AGH, **35**: 549–557.